Chapter 9

High Current Superconducting $\frac{1}{2}$-Cell Gun

9.1 Introduction

A superconducting energy recovery linac (SC-ERL) has been identified as the most efficient choice to generate and accelerate high current, high charge electron beam for the electron cooling project at RHIC. Electron cooling of ion beams is the main component of the next luminosity upgrade of the Relativistic Heavy Ion Collider (RHIC). Cooling ions (gold) at 100 GeV/nucleon requires very high average current ($>$ 200 mA) electron beam. A 20 MeV prototype SC-ERL is under construction as an initial R&D step towards the realization of the e^- cooler and future high current SC-ERLs. The prototype will consist of a $\frac{1}{2}$ cell SRF gun shown in Fig. 9.1 as an injector to the 20 MeV SRF linac comprised of a five-cell SRF cavity [111, 112], and a return loop back through the linac for energy recovery before the beam dump. This paper will focus on the design and optimization of the $\frac{1}{2}$ cell gun based on both RF issues and preservation of small transverse and longitudinal emittances. Table 9.1 shows some relevant parameters for the prototype SC-ERL which were used as inputs for the optimization procedure.

9.2 SRF Gun Design

Like any SRF cavity, the design of the gun is affected by the peak surface fields, avoidance of multipacting, access to efficient surface chemistry, minimization of welds at critical points, mechanical stiffness and complexity of manufacturing. High current beams along with high bunch charge pose a significant challenge in suppressing HOM wakefields and extraction of the large HOM power. Accelerating ampere CW class beams also require high power fundamental couplers (FPC) capable of delivering megawatts (MW) of power

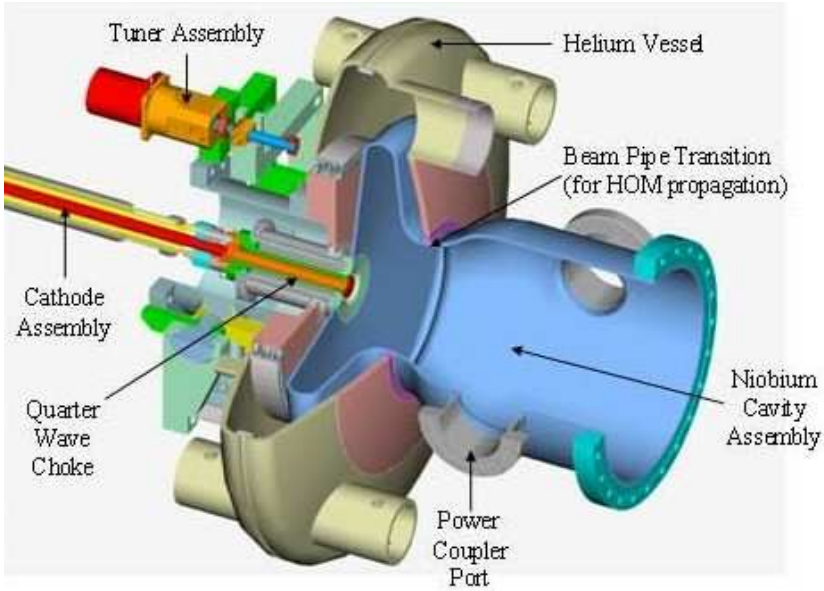

Figure 9.1: Conceptual 3D Graphic of $\frac{1}{2}$ cell SRF gun at 703.75 MHz with helium vessel, cathode insertion and tuner assembly (Courtesy AES).

which is non-trivial.

9.2.1 Cavity Shape

An initial design (1) was first proposed from the Rossendorf $\frac{1}{2}$ cell gun scaled to 703.75 MHz [113]. The cavity to beam pipe transition was enlarged to propagate all the lowest frequency HOMs. However, this design was inadequate to provide the required longitudinal focusing and emittance at the exit of the gun. A re-entrant shape (design 2) resulted from the modification of design 1 (right half-cell) to increase the longitudinal focusing and improve the overall emittance at the exit of the gun. This was achieved by shortening the effective cell length by reducing the beam pipe aperture and the wall angle and tuning for the frequency using the equator radius. However, coupling strongly to the fundamental mode ($Q_{ext} \sim 4 - 5 \times 10^4$) with a small beam pipe radius of 4 cm was not a viable option. The re-entrant shape may also pose problems relating to effective chemical treatment of the surface, multipacting issues and mechanical stability.

Several other designs (3-6) were developed as a result of shape optimization to reduce the effective cell length while keeping the beam pipe aperture $\geq 5cm$ and the wall angle $\geq 6.5^0$. The six different shapes that were considered are

Table 9.1: Parameters for the prototype SC-ERL used in simulations for optimization of the gun shape. A possible scenario with high charge and low repetition rate similar to the electron cooling case is also presented.

Parameter	High Current	High Charge
Injection energy [MeV]	2.5	2.5
Maximum energy [MeV]	20-40	20-40
Avg. beam current [A]	0.5	0.2
Repetition rate [MHz]	703.75	9.4
Charge/Bunch [nC]	1.4	10-20
Norm. emittance [mm.mrad]	1-3	30
Bunch length [cm]	1.0	3.0
Energy recovery efficiency	> 99.95 %	> 99.95 %

shown in Fig. 9.2, and detailed comparisons will be made in the following sections. Table 9.2 shows a comparison of some relevant RF parameters (peak fields and R/Q values) for the six designs.

Table 9.2: Comparison of RF parameters for the six different cavity shapes. The R/Q values are calculated using the accelerator definition. Note that the active cavity length is chosen from the cathode wall to the iris plane of the right half-cell of the gun.

Shape	R_{iris} [cm]	L_{cav} [cm]	R/Q [Ω]	E_p/E_a	B_p/E_a [$\frac{mT}{(MV/m)}$]
Design 1	7	10.1	100.0	1.20	2.88
Design 2	4	9.5	106.0	1.47	3.15
Design 3	6	10.0	102.4	1.27	2.96
Design 4	6	10.0	102.8	1.33	2.69
Design 5	5	9.5	95.0	1.43	2.96
Design 6	6	9.5	92.1	1.42	2.88

9.2.2 HOM Power

High current along with high bunch charge beams dissipate large amount of power into HOMs, which has to be extracted outside the cryogenic envi-

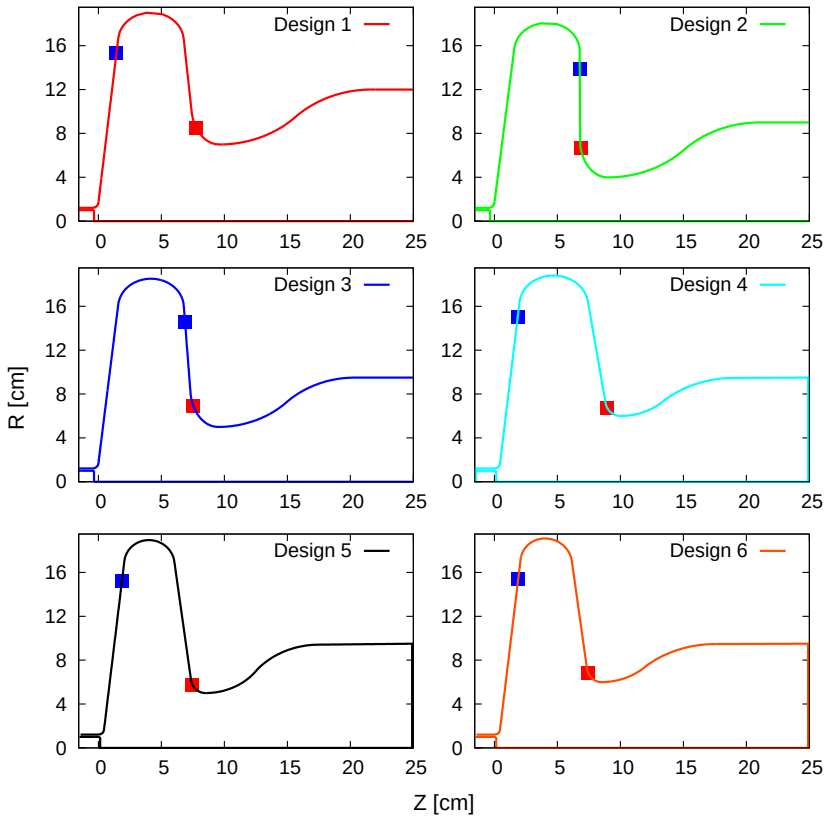

Figure 9.2: Six different cavity shapes used for comparison based on both RF and beam dynamics issues for the 703.75 MHz SRF gun. The red and blue solid squares represent the location of the peak electric and magnetic fields in the cavity respectively.

ronment. Beam pipe ferrite absorbers will be placed in the warm section to absorb this HOM power for modes above the cut-off frequency of the beam pipe. The average power dissipated by a beam traversing a structure is given by

$$P_{HOM} = k_{||} Q_b I_b \tag{9.1}$$

where $k_{||}$ is the geometrical loss factor of the structure. The loss factors for the six designs are calculated using ABCI [87, 88] and are shown in Fig. 9.3. The loss factors are quite similar ($\sim 0.7\ V/pC$), and the total HOM power dissipated is approximately 0.5 kW for a 500 mA beam current and 1.4 nC bunch charge.

Note that the loss factors shown in Fig. 9.3 were calculated for ultra relativistic particles ($\beta = 1$) and are assumed as the upper limits for the case with

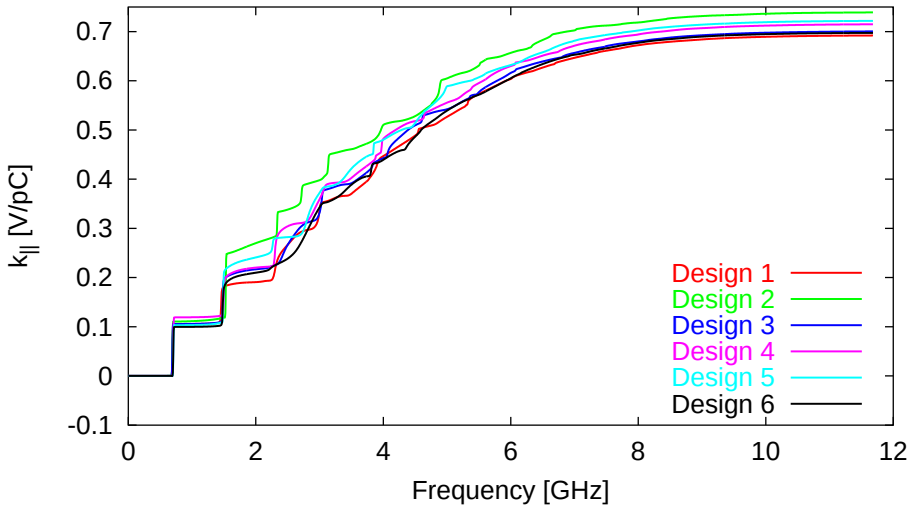

Figure 9.3: Integrated longitudinal loss factor calculated by ABCI for the six different designs under consideration.

$\beta < 1$ (see appendix A).

9.2.3 Multipacting

As any RF cavity the gun also is prone to multipacting, a resonant electron multiplication caused by electrons emitted from the surface. The primary electrons impact back on the surface emitting secondary electrons. If they satisfy the resonant condition with a secondary electron yield (SEY) larger than 1, it can lead to an avalanche. This will lead to absorption of RF power and thermal breakdown of the superconducting surface.

The Helsinki 2D code, MultiPac 2.1 [99, 100] is used to calculate the field levels at which multipacting can be onset for the six designs. Fig. 9.4 shows the counter function representing the total number of electrons (primary and secondary) and corresponding impact energies as a function of peak electric field. The total number of electrons after a given number of impacts normalized to the average secondary emission coefficient corresponding to the impact energy (enhanced counter function) is shown in Fig. 9.5 as a function of peak electric field. An enhanced counter function larger than 1 represents an onset of multipacting at that field level. Fig. 9.5 shows two main regions of interest, one at low surface fields ($< 5MV/m$), and the other at high surface fields ($>$ 30 MV/m). The impact energies near 0.5 MV/m are considerably high ($\gg$ 2 keV) and the impact energies near 33 MV/m are very low ($<$ 30 eV).

For both impact energies, the corresponding SEY for niobium is smaller than 1. Therefore, the enhanced counter function is much smaller than 1 as seen from Fig. 9.5, thus making multipacting very unlikely. The electron trajecto-

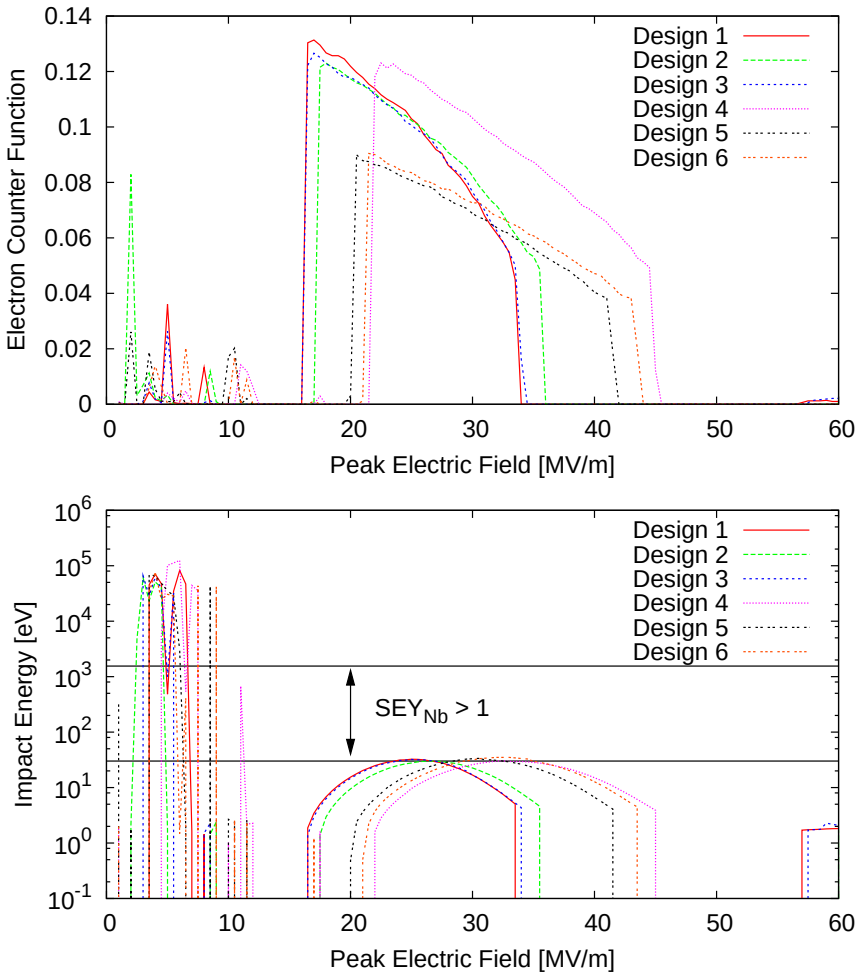

Figure 9.4: Top: The electron counter function representing the total number of free electrons after a given number of impacts (20) as a function of peak electric field. Bottom: The final impact energy of the electrons surviving the maximum number of impacts (20) as a function of peak electric field.

ries for the two field regions are shown in Fig. 9.6. The trajectory in the low field region (∼5 MV/m) does not stabilize and drifts radially. The electrons are lost after approximately 40 impacts. The trajectory at high field region (∼33 MV/m) exhibits stable two point multipacting.

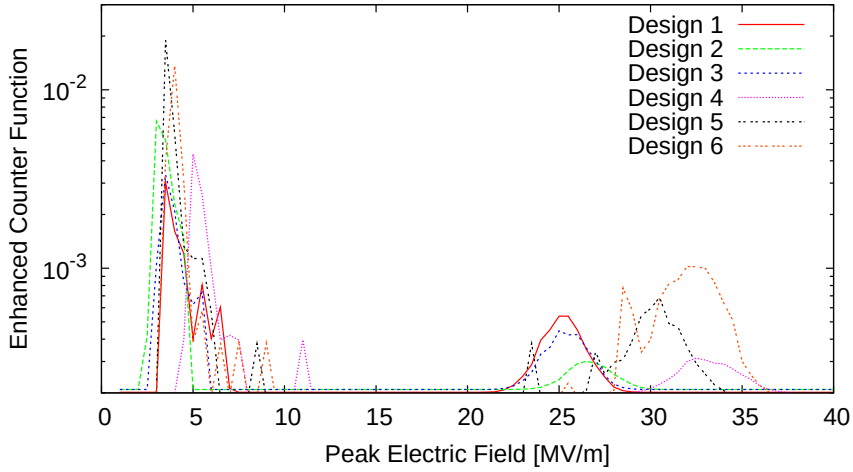

Figure 9.5: The enhanced counter function which represents the number of secondary electrons after a given number of impacts normalized to the secondary emission coefficient corresponding to the impact energies plotted as a function of electric field.

9.3 Beam Dynamics

In addition to RF and mechanical requirements, the preservation of very low emittances and energy spread due to space charge forces puts strict constraints on the gun shape. For meaningful calculations of longitudinal and transverse beam emittances, simulations for the six designs are preformed using PARMELA [114, 115] for a prototype ERL system comprising of a 2 MeV SRF gun, a Z-bend injection merging optics [116], and a 20 MeV linac [111, 112]. The longitudinal electric field of the gun for beam simulations are calculated using SUPERFISH [117].

9.3.1 Longitudinal Focusing

The beam acquires an energy spread due to longitudinal space-charge forces giving the head of the bunch a higher energy relative to the rest of the bunch. A large energy spread can lead to adverse affects on the beam quality. To counter this energy spread, the bunch phase is placed before the peak in the energy-phase curve to achieve longitudinal focusing. This curve is dependent on the effective length of the gun (including the field penetration into the beam pipe), the electric field intensity, and the degree to which the cathode is recessed. The energy vs. initial phase of the emitted electrons calculated for

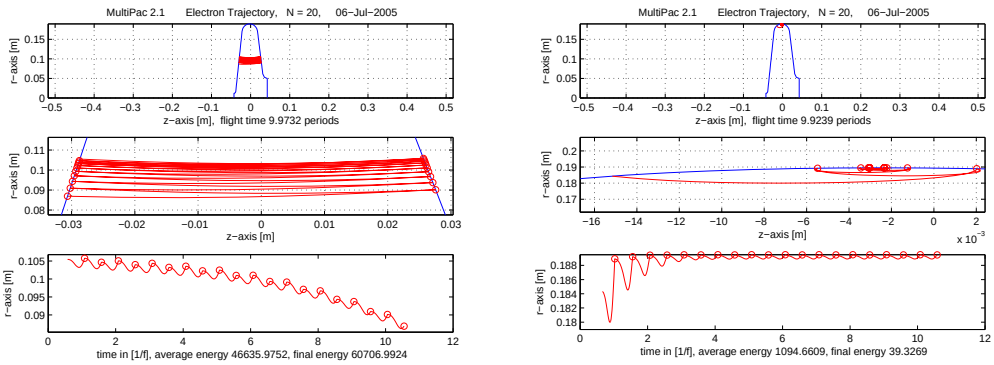

Figure 9.6: Left: Electron trajectory calculated for a peak electric field of approximately 5 MV/m. The trajectory drifts radially and does not stabilize. The electrons are lost after approximately 40 impacts. Right: Electron trajectory calculated for a peak field of approximately 33 MV/m which shows a stable two point trajectory but no multipacting is expected due to impact energies smaller than 30 eV.

the six designs is shown in Fig. 9.7. Design 2 & 5 show a significant positive slope compared to the others, thus providing a larger phase window for placing the bunch and provide effective longitudinal focusing to achieve the smallest energy spread.

The beam dynamics calculations in the following were made with a bunch charge of 1.4 nC, emitted from a cathode spot size of 5.0 mm diameter. The launch phase was chosen to be 25° as a result of optimization of the beam dynamics of photoinjectors with space charge [118]. A sufficiently large initial phase is required to provide adequate field on the cathode for electron emission and acceleration. Furthermore, to minimize chromaticity, the launch phase should be placed before the maximum energy gain on the positive slope of the energy-phase curve. For designs 2 and 5 the initial phase of 25° results in a minimum energy spread. The bunch distribution was uniform in both transverse and longitudinal directions. Fig. 9.8 shows the energy spread as a function of longitudinal position for the different gun shapes.

The electrons start from the cathode from rest. Therefore, a high field on the cathode is necessary to rapidly accelerate the high charge bunches to avoid emittance dilution due to space charge forces. Fig. 9.9 shows a schematic of two cases with a recessed cathode (left) and a cathode inserted 3mm towards the cavity wall (right). From Fig. 9.10 one can see that ratio of E_{cath}/E_{acc} is significantly larger when the cathode is not recessed with respect to the

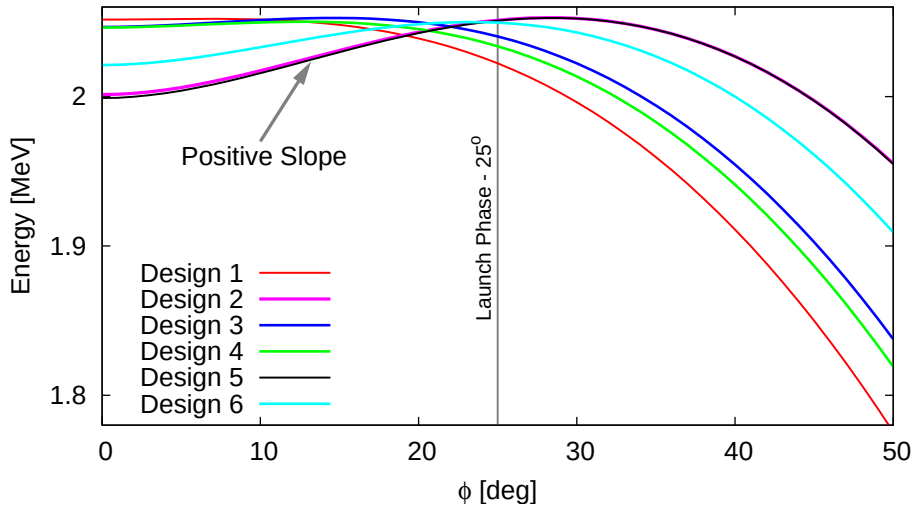

Figure 9.7: Energy of the electrons plotted as a function of initial phase for the six designs. Positive slope indicating an effective longitudinal focusing required for maintaining a small energy spread.

cavity wall. This high field near the cathode region is crucial to accelerate the electrons immediately after leaving the cathode to counteract space charge effects.

9.3.2 Transverse Emittance

Transverse focusing of the high-charge electron bunch and matching it to the invariant beam envelope [119, 120] is critical to achieve extremely small transverse emittance from the gun. This requires under certain conditions a recessed cathode, a solenoidal magnetic field or combination of the two. The evolution of vertical emittance through the SRF gun (recessed cathode), a nominal merging system, and a 20 MeV linac is seen in Fig. 9.11. Although, all guns show small emittances, designs 2 & 5 are significantly better. Table 9.3 lists loss factors, transverse emittances and energy spreads for the six designs.

The actual amount of recess must be determined by optimizing the effects of the larger electric field on the cathode which favor no recess, and transverse focusing which favors a recess. Fig. 9.12 shows the longitudinal and transverse emittances through the same prototype system, but with a simplified injection system (without bends). For each recess position of the cathode, the initial spot size, bunch length, and the solenoids were adjusted to minimize

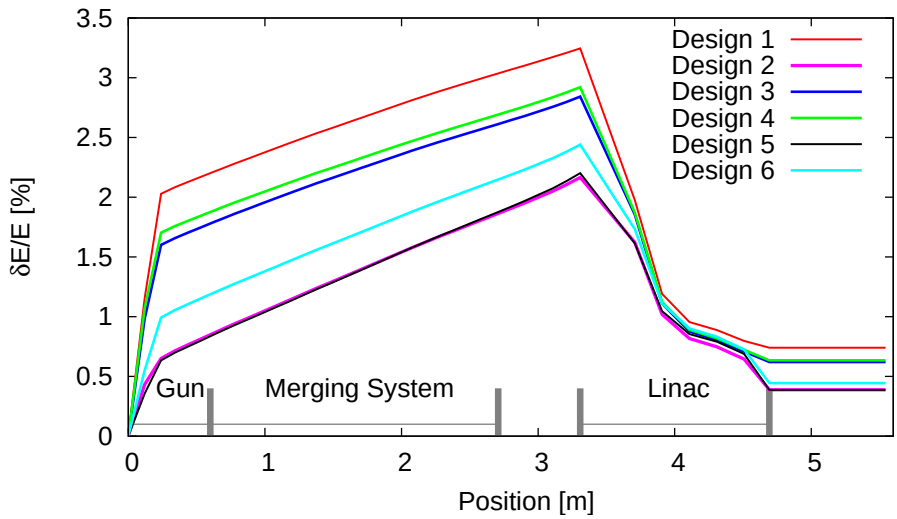

Figure 9.8: Energy spread of the electron beam calculated by PARMELA for a system with the gun, merging system, and a 20 MeV linac for the six different designs.

emittance at the exit of the Linac. It can be seen from Fig. 9.12 that position of the cathode with respect the cavity wall has a strong influence on both longitudinal and transverse emittances. Therefore, the cathode positions of -1 ± 0.5 mm with respect to a cavity wall seems to be an optimal region, and an adjustable cathode stalk is proposed for the prototype design to determine the best insertion length with beam. The launch phase for a fixed recess was varied $\pm$ 5° which had a weak effect on the final emittances.

9.4 Final Design and Issues

All six designs exhibit similar RF characteristics, but designs 2 and 5 show significantly better emittances in both longitudinal and transverse planes. Design 5 is prefered for its better mechanical properties, and its accessibility for a more effective surface treament due to larger wall angles. Additionally, a larger iris radius in design 5 is preferable to achieve strong FPC coupling. The geometrical parameters for design 5 are shown in Table 9.4. Issues relating to HOM damping and the FPC coupler will be discussed using design 5 in the following sections.

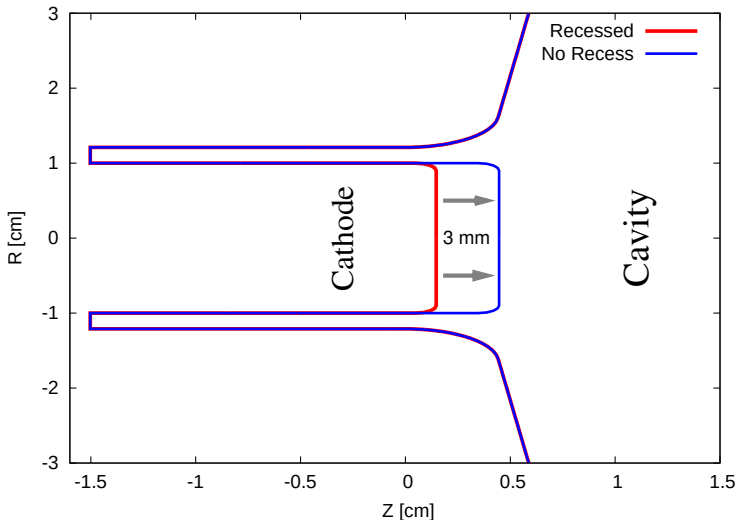

Figure 9.9: Graphic of the recessed and non-recessed cathode with the $\frac{1}{4}$ wave choke for RF isolation near the cathode region. The choke will be at an elevated temperature compared to the SRF gun.

9.4.1 Transition Section

It is important to damp all HOMs to avoid single bunch and multi-bunch effects which can degrade the beam quality and possibly lead to instabilities. It was initially proposed to enlarge the beam aperture similar to the five-cell linac cavity [112] to propagate all HOMs down to the lowest frequency, and damp them using beam pipe ferrites. HOM loop couplers were unfavorable due to their low power handling capability and their resonant nature leading to a high probability of failure for high current operations. The impedance spectrum of monopole and dipole modes are shown in Fig. 9.13 for the SRF gun and is compared to the case with the enlarged beam pipe. Fig. 9.14 shows a schematic of the gun with and without an enlarged beam pipe aperture of 19cm. The density of HOMs is quite small below 6 GHz beyond which the cavity modes are above the beam pipe cut-off. Also, the increase in the beam pipe aperture to 19 cm is only effective in propagating a subset of the trapped modes. Further increase in aperture may not be feasible without compromising beam emittances. Therefore, the choice of an enlarged beam pipe was avoided at the cost of having a few extra undamped modes. This allows one to bring the FPC closer to the cavity and couple strongly without requiring to penetrate deep into the beam pipe. The straight beam pipe also allows one to bring the first solenoid closer to the gun to improve the beam emittances, as well as

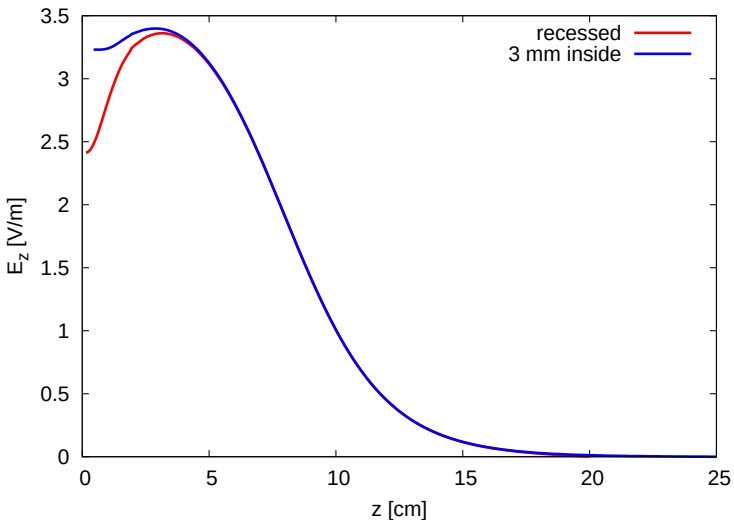

Figure 9.10: The magnitude of the electric field plotted a function of longitudinal position for the recessed and non-recessed cathode cases. The non-recessed cathode shows a field enhancement in the proximity of the cathode which is important to accelerate the electrons immediately to counteract space charge effects.

simplify several engineering issues.

Fig. 9.13 also shows a train of Dirac-δ functions (black spikes) representing the harmonics of the bunch repetition frequency of 703.75 MHz. The harmonics are well separated from the high Q undamped modes which allievates the need for damping. However, if the repetition rate is much smaller than 703.75 MHz, the number of harmonics will consequently become large. This may cause an inevitable overlap with one or more of the cavity resonances and dissipate large amounts of beam power into the HOMs. A tuning mechanism (possibly a HOM tuner) may become necessary to detune the HOM frequencies to avoid resonant excitation for lower repetition rates.

The bunches emitted from the cathode can also exhibit variation in amplitude and timing jitter caused by the amplitude and timing jitter of the laser. The modulation is usually random in nature and will induce a change in the frequency spectrum of the harmonics. It is important to understand the spectral behavior of the beam harmonics in the presence of the modulation to avoid any overlap with the cavity resonances. The spectral power density of a modulated current of pulse shape $p(t)$ is derived in appendix B for general uncorrelated variables. For simplicity, we will assume that the harmonics represent a infinite train of Dirac δ functions ($\hat{p}(\omega) = 1$) separated by T_0. The

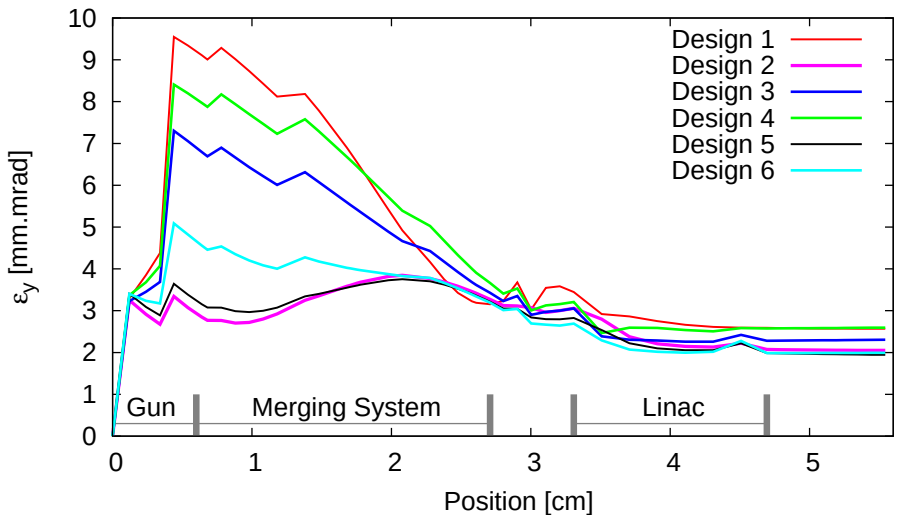

Figure 9.11: Vertical emittance calculated by PARMELA for the six designs in a beam line with the gun, merging system and 20 MeV linac.

amplitude modulation and time jitter can be included into the beam current as

$$I(t) = \sum_{n=-\infty}^{\infty} a_n \delta(t - nT_0 - \epsilon_n) \tag{9.2}$$

where a_n and ϵ_n are random uncorrelated variables. Assuming that a_n and ϵ_n have uniform distributions with rms σ_a and σ_ϵ respectively, the spectral power can be calculated from Eqs. E.13 and E.14 and is given by

$$\begin{aligned} P(\omega) &= \frac{2\pi}{T_0^2} \underbrace{\left[\frac{\sin(\sqrt{3}\omega\sigma_\epsilon)}{(\sqrt{3}\omega\sigma_\epsilon)}\right]^2}_{envelope} \sum_{m=-\infty}^{\infty} \underbrace{\delta\left(\omega - \frac{2\pi m}{T_0}\right)}_{harmonics} \\ &\quad + \frac{1}{T_0} \underbrace{\left[\left(1 - \left[\frac{\sin(\sqrt{3}\omega\sigma_\epsilon)}{(\sqrt{3}\omega\sigma_\epsilon)}\right]^2\right) + \sigma_a^2\right]}_{baseline} \end{aligned} \tag{9.3}$$

From Eq. 9.3, it can be seen that the power spectrum has two components. The first component represents the harmonics of the bunch repetition frequency given by a Dirac comb suppresed by a sinc envelope. The second component is a "baseline" sinc function independent of the harmonics and can result in large HOM power for large σ_ϵ and σ_a. Fig. 9.15 shows a simulation

Table 9.3: Beam dynamics parameters for the six designs under consideration as shown in Fig. 9.2.

Shape	$k_{\|\|}$ [V/pC]	$k_{\perp}$ [V/pC/m]	ϵ_y [mm.mrad]	$\delta E/E$
Design 1	0.692	49.1	2.569	7.4 %
Design 2	0.7397	31.42	2.053	3.9 %
Design 3	0.7011	31.62	2.306	6.2 %
Design 4	0.7155	32.3	2.595	6.3 %
Design 5	0.7225	31.74	1.944	3.86 %
Design 6	0.6981	32.25	1.993	4.4 %

Table 9.4: Cavity geometrical parameters using the parametrization decribed in Ref. [68] of the right half-cell for design 5. The left wall angle of the gun was maintained at 6.5° with a cathode radius of 1.46 cm.

Parameter	Right Half-Cell
Frequency	703.75 MHz
Iris Radius, R_{iris}	5.0 cm
Wall Angle, α	6.5°
Equatorial Ellipse Ratio, $R = \frac{B}{A}$	1.1
Iris Ellipse Ratio, $r = \frac{b}{a}$	1.2
Dist. from cav. wall to iris plane,	1.0 cm
Active cavity Length, L	8.5 cm
Dist. from center to equator end	18.95 cm
Avg. Beta, $< \beta = \frac{v}{c} >$	0.587

of the effect of amplitude modulation (10%) and timing jitter (10 ps) with uniform random distributions and is compared to the analytical expression. The finite number of frequency samples in the simulation result in the sinc like behavior of the harmonics (see Eq. E.12).

It is of interest to estimate the additional voltage induced in a given trapped mode due to the beam fluctuations. An approximate expression for the induced voltage for a simple statistical model for the fluctuations is derived in appendix C. Assuming a bunch length of 1 cm, $\sigma_a = 1\%$, $\sigma_\epsilon = 1$ps, and a $Q_{ext} \approx 10^8$, the ratio of the voltage induced due to fluctuations to the accelerating voltage ($\sim$ 2 MV) for the first longitudinal trapped HOM (TM_{011}) is approximately 9×10^{-3}. These modulation criteria for σ_a and σ_ϵ are easily feasible with

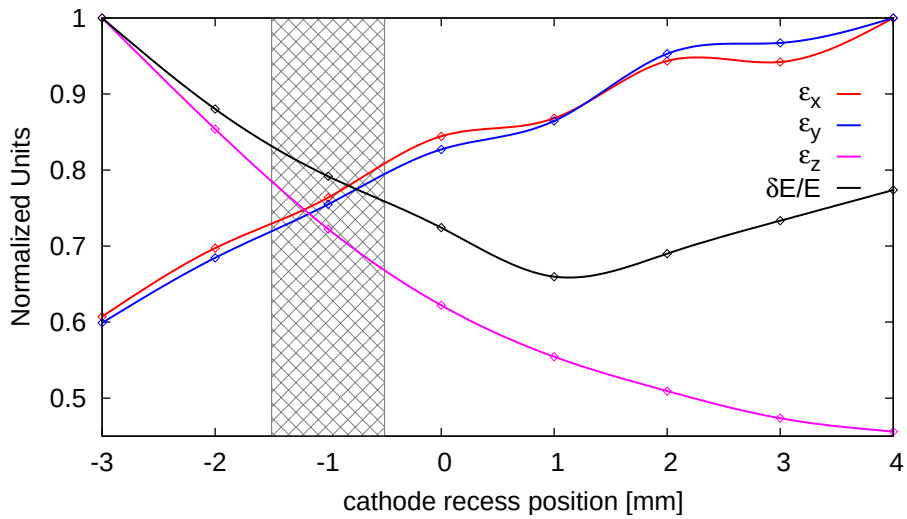

Figure 9.12: Longitudinal and transverse emittances at the end of a 20 MeV Linac for different positions of the cathode in SRF gun (results of PARMELA simulations). The energy of the e^- at the exit of the gun was fixed. Note that all emittances are normalized and the solid lines are spline fits to the simulation points.

current technologies. However, the induced parasitic voltage is significant, and the contribution to the energy spread is comparable to that of space charge effects. Therefore, tighter tolerences will be required to suppress the effects of laser fluctuations. Furthermore, the presence of a strongly coupled FPC, although not matched to HOM frequency, is expected to damp the HOMs ($Q_{ext} \ll 10^8$), and therefore relax the modulation criteria.

9.4.2 Fundamental Power Coupler

Another critical component of the SRF gun is the design of FPC. The SRF gun is being designed to generate a 2 MeV beam with an average current of 500 mA or larger. Therefore, the average RF power required is ≥ 1 MW, thus requires very strong coupling ($Q_{ext} \sim\ 4-5\times10^4$). Several options of electrical and magnetic coupling were considered, and a coaxial coupler with a "pringle" shaped electrical tip was found to be an effective choice. The pringle shape (originally designed for the Cornell ERL injector [103]) with a contour radius of the beam pipe is used to maximize coupling while minimizing wakefield effects. Fig. 9.16 shows a graphic of the SRF gun with the dual fundamental couplers (FPCs) to couple RF power into the gun.

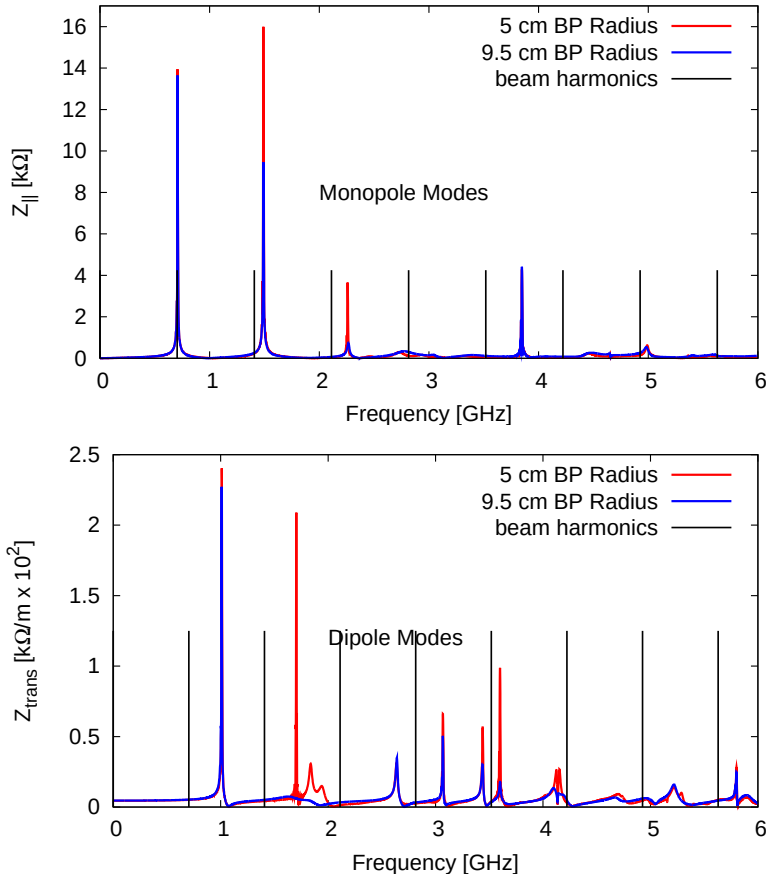

Figure 9.13: Broadband impedance spectrum calculated using ABCI [87, 88] for longitudinal (monopole like) and transverse (dipole like) modes for the two different beam pipe transitions. The black δ functions represent the harmonics of the bunch repetition frequency.

The beam pipe radius and the distance of the FPC to the cavity is fixed due to beam dynamic issues and engineering constraints. Therefore, the following geometrical aspects of the coupler were studied to increase coupling while minimizing the penetration of the inner conductor to reduce coupler kicks and wakefields. Note that the Q_{ext} for the optimization scans were calculated from the 3 db bandwidth of the transmission coeffcient (S_{21}) using the frequency domain of Microwave studio [102, 121].

- The intersection of the outer conductor and beam pipe was blended as shown in Fig. 9.17. A scan of Q_{ext} as a function of the blend radius is plotted in Fig. 9.17. The two curves represent scans performed with

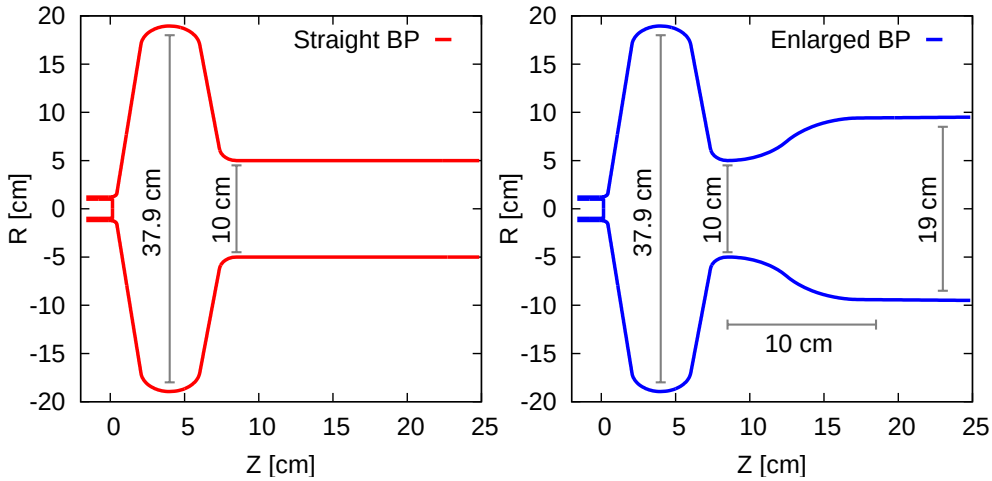

Figure 9.14: Graphic of the two different transition sections considered for the SRF gun. The straight beam pipe without enlargement is preferred due to the simplicity in manufacturing at the cost of a few undamped modes.

two different pringle radii (25 cm, 30 cm) which exhibit approximately linear behavior. A larger radius is prefered, but the actual radius will be constrained by the helium vessel and tuning fixtures.

- An elliptical pringle was found to provide larger coupling than a circular pringle. This is partially due to the geometry of the outer conductor and the beam pipe intersection. The optimized semi-major ($x_r \approx 36$ mm) and semi-minor ($y_r \approx 27$ mm) axes of the pringle cross section and the contour of the elliptical pringle are shown in Fig. 9.18. A scan of Q_{ext} as a function of the transverse dimensions of the pringle is shown in Fig. 9.19. A larger x_r is prefered, but it cannot exceed the radius of the outer conductor due to clearance for assembly of the FPC in clean room conditions.

- The thickness of the pringle tip was also varied to study the effect on coupling. Fig. 9.20 shows scans of Q_{ext} as a function of the tip thickness for two different pringle radii (25 mm and 30 mm). The thickness has a stronger influence on Q_{ext} for a larger pringle radius. A thinner pringle is prefered, but it should be mechanically rigid.

- With the most optimized geometry of the coupler, the penetration of the inner conductor into the beam pipe was varied to achieve the required coupling. Fig. 9.21 shows a a scan of the Q_{ext} as a function of

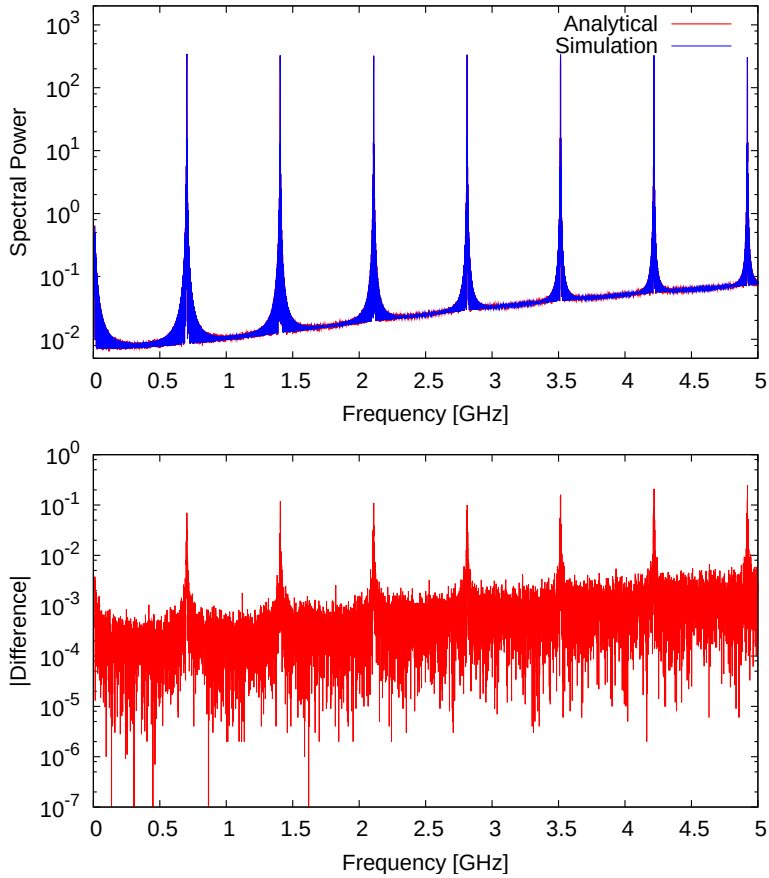

Figure 9.15: Top: Simulation of the frequency spectrum of the harmonics of the bunch repetition frequency in the presence of timing jitter ($\sigma_\epsilon = 10$ ps) and amplitude modulation ($\sigma_a = 10$ %) compared to Eq. E.12. Bottom: Absolute value of the difference between analytical formula and simualtion.

the penetration depth. With the geometric modifications, the required $Q_{ext} \sim 4 - 5 \times 10^4$ can be achieved with penetration of $\leq$ 2mm which is significantly less than previously required 10 mm [107].

The presence of a FPC can lead to a non-zero transverse field on-axis resulting in a kick to a bunch traversing the structure. Since, the energy of the beam is relatively low ($\sim$ 2 MeV), the effect of the kick on the bunch can be significant. One of the remedies to minimize the transverse kick is to add a symmetric coupler to cancel the effect. On top of minimizing the kick, the average power through coupler would be also halved, thus relaxing the power handling of the FPCs. However, symmetric couplers are prone to

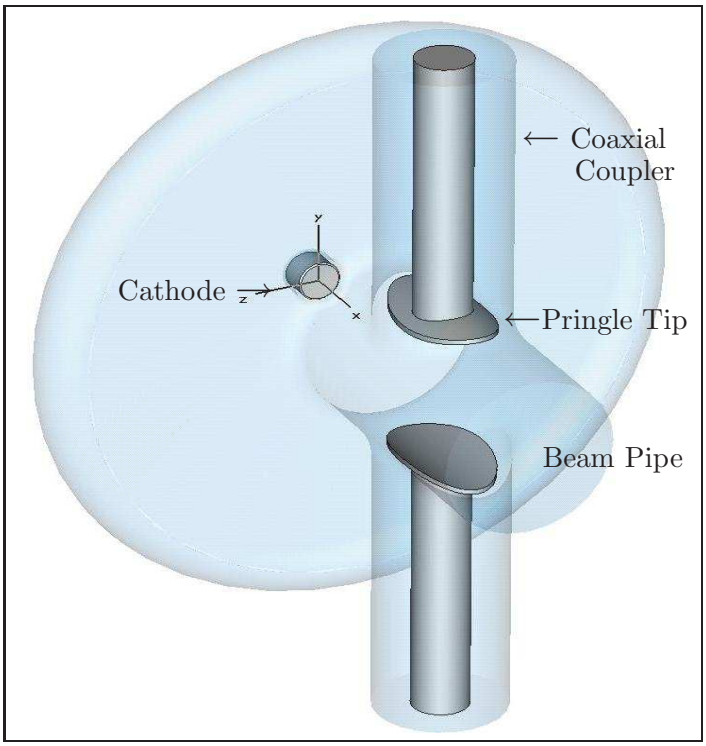

Figure 9.16: 3D graphic of the 703.75 MHz SRF gun with the dual FPCs with an optimized "pringle" tip.

manufacturing and alignment errors, but the transverse kick is significantly smaller compared to a gun with a single coupler. For a dual coupler geometry, an asymmetry in the penetration or a phase mismatch between the coaxial lines can result in a transverse kick. The transverse fields for both cases are shown in Fig. 9.22 and the respective transverse kicks are computed using an approach similar to described in Ref. [103].

The transverse "kick factor" is simply given by

$$\delta_t = \frac{\int (E_y + v_z B_x) dz}{\int E_z dz} \tag{9.4}$$

which can be numerically evaluated. The normalized emittance growth due to the time dependent RF kick can be estimated using the formula derived in Ref. [105] which is given by

$$d\epsilon_n = \sigma_t \frac{2\pi\sigma_z}{\lambda_{RF}} \frac{eV_{acc}}{E_0} \left|\mathrm{Re}(\delta_t)\sin\phi_0 + \mathrm{Im}(\delta_t)\cos\phi_0\right| \tag{9.5}$$

where ϕ_0 is the bunch phase with respect to the RF, E_0 is the rest mass of

the e^-, σ_t and σ_z are the transverse and longitudinal beam sizes, and V_{acc} is the voltage of the accelerating gap. Table 9.5 shows the kick factors and relative emittance growths for the two cases with transverse RF fields. In both cases, the emittance growth estimates are quite small compared to space charge induced growth.

Table 9.5: Transverse kick and normalized emittance growth for a two-coupler scheme with an asymmetry in penetration depth and phase offset respectively.

Asymmetry	Kick	$d\epsilon_n/\epsilon_n$
Tip Penetration (1 mm)	(-6.1 - 5.0i)$\times 10^{-5}$	$< 3\%$
Phase Offset (1 deg)	(8.4 - 5.9i)$\times 10^{-5}$	$< 3\%$

9.4.3 Cathode Isolation & Design Issues

The addition of a replaceable and variable laser photo-cathode (for example cesium potassium antimonide) in ultra clean superconducting environment adds to the overall complexity of design. Some of the main issues are as follows

- Providing a demountable joint that is thermally isolated from the cavity to minimize heat load into the liquid helium environment.
- The demountable joint also carries a large RF current which must be prevented from developing large losses in the normal-conducting joint.
- Avoid strong multipacting in the cathode stalk
- A separate liquid nitrogen channel is required to remove the heat generated in the cathode.
- The cathode material should be replaceable without breaking the vacuum while keeping the gun at superconducting temperature.

A simple approach involving a multiple quarter wave choke joint is being designed for RF isolation of the demountable cathode insertion. Triangular groves on the choke joint are under investigation to suppress multipacting by effectively reducing the SEY by geometric means. Initial tests on a copper prototype show no evidence of strong multipacting for the proposed design [123].

The structure of the cathode current stimulated by the laser also can be a source of abundant harmonics causing extra losses in the choke. Since, the

choke is only a short for the fundamental mode (703.75 MHz), it must be designed carefully to avoid any resonances that will coincide with the harmonics of the bunch repetition frequency and result in large losses [124].

9.5 Ideas for a $1\frac{1}{2}$-Cell Gun for e^- Cooling

For e^- cooling, the injection energy is set at ∼5 MeV. The beam requirements are outlined in Table 6.1. The injector gun for e^- cooling will also be a all niobium SRF gun with $1\frac{1}{2}$ cells. Under the assumption of high gradient (25-50 MV/m), it was shown that a longer first $\frac{1}{2}$ cell ($\sim 0.6\lambda/2$) was optimum for final longitudinal and transverse emittances [125, 126]. Similar to the $\frac{1}{2}$-cell gun for the prototype, an optimization of the cell shape is underway for the $1\frac{1}{2}$ cell gun. This is an iterative procedure to optimize both RF issues and final beam emittance. A few initial designs with a half-cell length of $\lambda/2$ and different iris radii were developed as a starting point as shown in Fig 9.23.

The presence of a second cell with only one beam pipe opening poses a challenge of possible trapped HOMs which are now twice as many compared to the $\frac{1}{2}$-cell gun. However, the addition of the second cell relaxes the need for having a small iris, and allows one to use this as tuning parameter for better HOM damping. The goal of the iterative procedure is to arrive at a final iris radius and cell lengths of the two cells to have the best possible HOM damping as well as the small final beam emittances. The general procedure will follow the steps outlined below:

- Iris radius optimization
  - Study of HOM spectrum and impedances as function of R_{iris}
  - Frequecies of HOMs and respective cut-off frequecies for different radii
- Beam pipe transition
  - Propagate of modes below cut-off of the final R_{iris}
  - Strong fundamental power coupling without large penetration of coaxial attenna
- Determine optimum length of cell lengths (l_1 and l_2)
  - Maximize the positive slope on the energy-initial phase curve for longitudinal focusing

  - Minimize transverse emittances

- Determine optimum cavity geometrical parameters using peaks field, R/Q, mechanical stability and other relevant issues [1].

Other issues like fundamental power coupler and cathode stalk design can be directly adapted from the $\frac{1}{2}$-cell design.

9.6 Conclusion

A prototype SC-ERL is underway to test various components and physics issues to demonstrate the feasibility of ampere class ERLs. A $\frac{1}{2}$ cell SRF gun with diamond amplified photo-cathode is chosen as the injector to the SC-ERL. Six potential designs for the $\frac{1}{2}$ cell gun have been presented and several RF, mechanical and beam dynamics issues were used in the optimization of the final choice of the gun shape. Design 5 was found to adequately satisfy RF and mechanical constraints as well as provide longitudinal and transverse focusing to combat space charge forces thus resulting in a low emittance beam with a small energy spread. Issues related to multipacting, cathode insertion, and laser stability were also presented. A general procedure for the development of a $1\frac{1}{2}$-cell for e^- cooling is outlined with some initial designs under progress.

[1] The cavity geometrical parameters like the ellipse ratios have been determined from an intial optimization run.

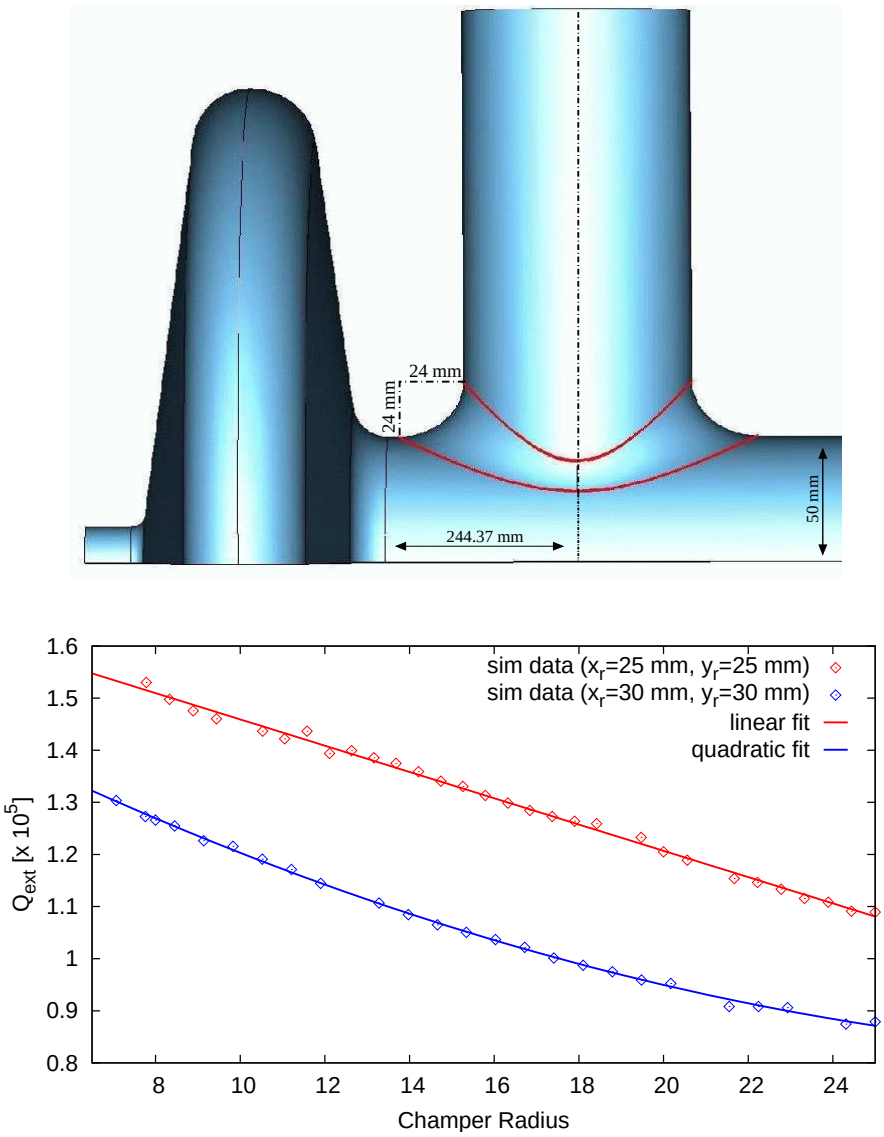

Figure 9.17: Top: Graphic of the symmetric top-half of the SRF gun with the FPC outer conductor intersection to the beam pipe. This intersection is blended using an arc to couple stronger to the fundamental mode without increasing the entire beam pipe radius. Bottom: Q_{ext} plotted as a function of the blend radius of the edge between FPC and the beam pipe. The two curves represents the scan with two different pringle radii.

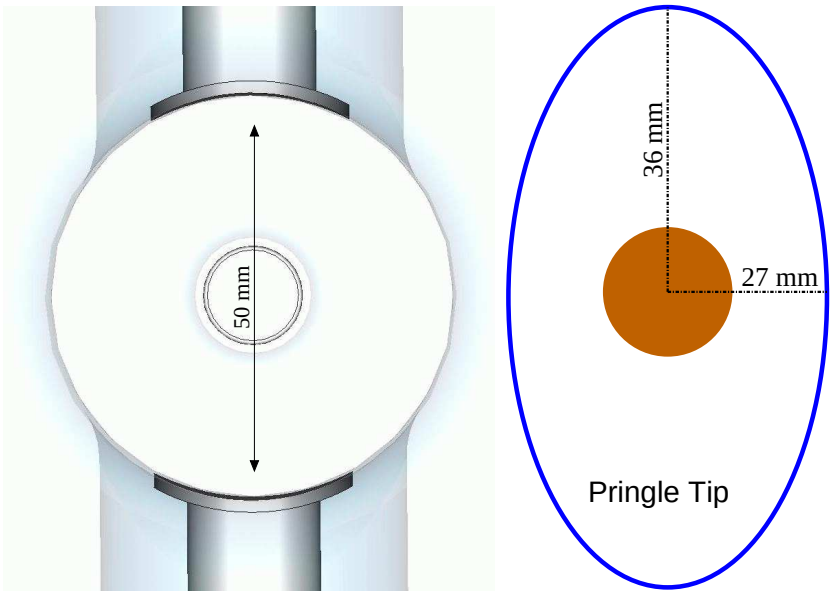

Figure 9.18: Left: A longitudinal cross section of the SRF gun and the coupler which shows the contour of the pringle tip. Right: The transverse dimensions of the elliptical pringle optimized for maximum coupling.

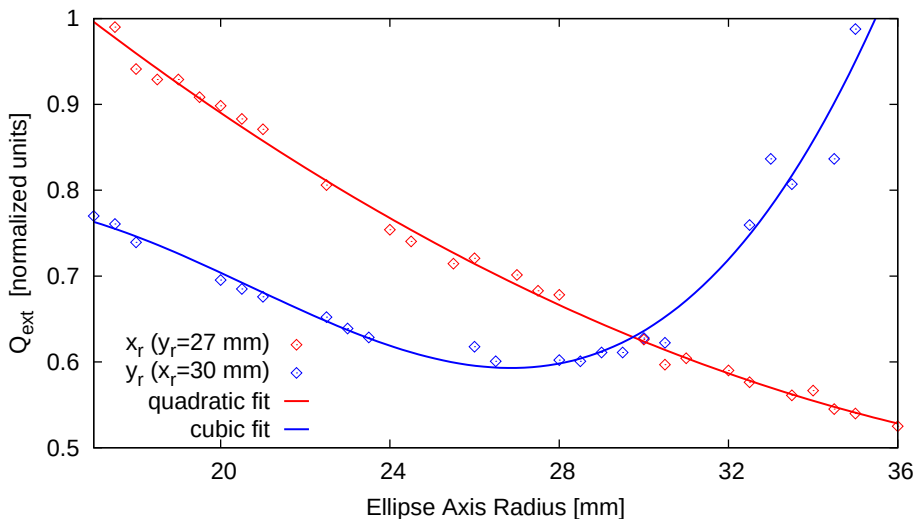

Figure 9.19: A scan of Q_{ext} as a function of the transverse dimensions of the elliptical pringle. The solid lines are quadractic and cubic fits for x_r and y_r respectively. The y-axis is normalized to compare the effect of both transverse dimensions on the same scale.

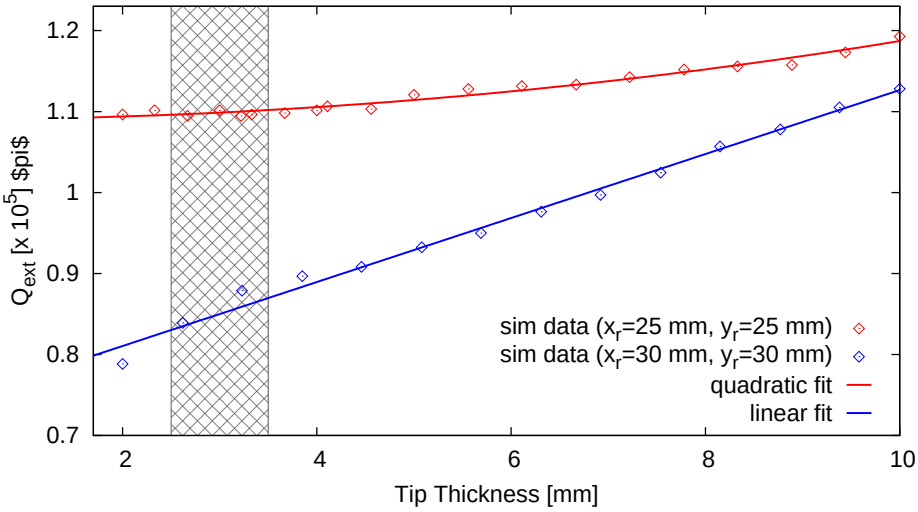

Figure 9.20: A scan of Q_{ext} as a function of the thickness of the tip for two different pringle radii. The solid lines are fits to the the calculated Q_{ext} points which are approximately linear.

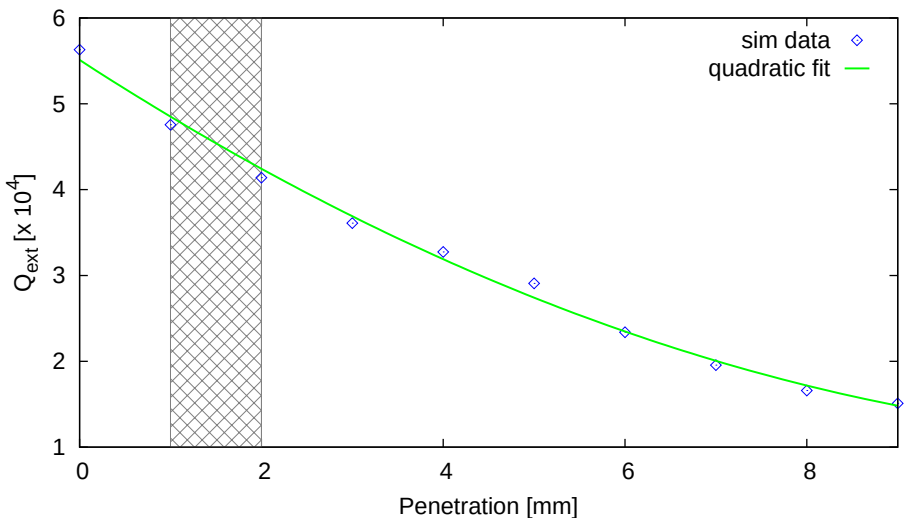

Figure 9.21: A scan of Q_{ext} as a function of the penetration of the tip in to the beam pipe. The solid line is a quadratic fit to the the calculated Q_{ext} points. The shaded area shows the expected penetration to achieve the required Q_{ext}.

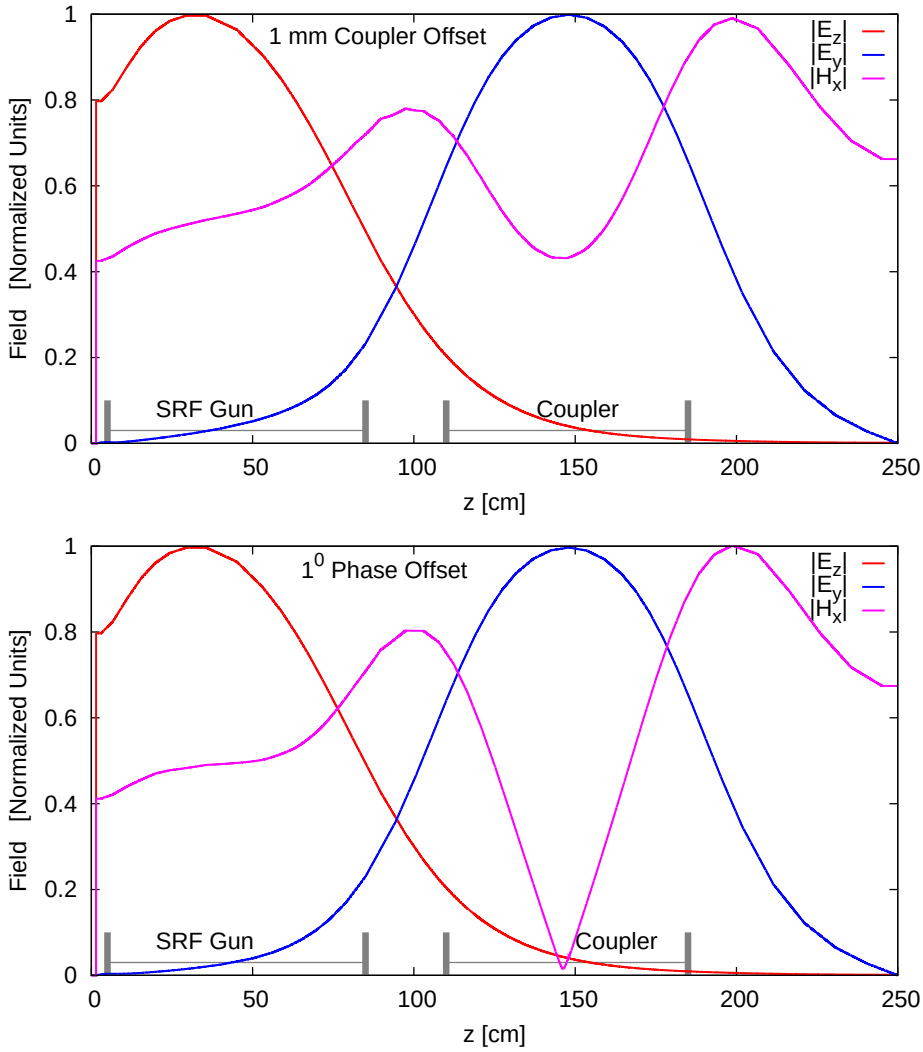

Figure 9.22: Longitudinal and transverse fields on-axis of the SRF gun due to 1 mm asymmetry in the coupler penetration between the dual couplers (top) and 1^0 phase offset between the dual couplers (bottom) [104].

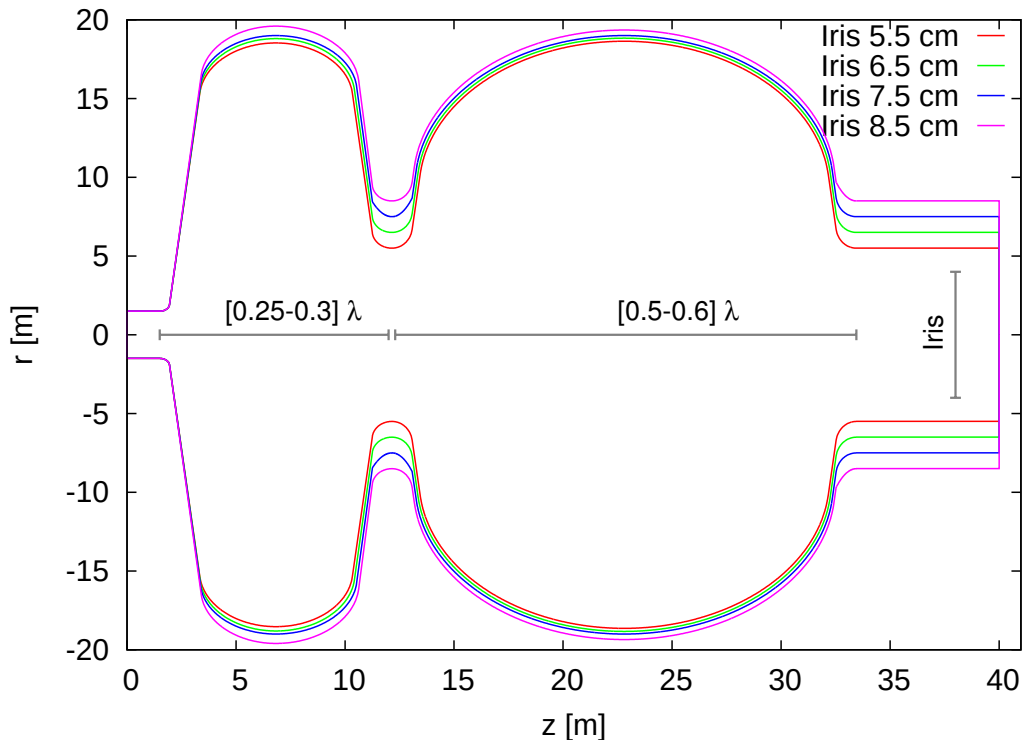

Figure 9.23: Initial design of the $1\frac{1}{2}$-cell gun designs with half-cell length of $\lambda/2$, and different radii (5.5-8.5 cm) for e^- cooling injector.